J. Fluid Mech. (1997), *vol.* 339, *pp.* 287–307. Printed in the United Kingdom

Transverse velocity increments in turbulent flow using the RELIEF technique

By A. NOULLEZ[1], G. WALLACE[2], W. LEMPERT[2], R. B. MILES[2] AND U. FRISCH[1]

[1] Observatoire de la Côte d'Azur, BP 4229, 06304 Nice Cedex 4, France
[2] Department of Mechanical and Aerospace Engineering, Princeton University, Princeton, NJ 08544, USA

(Received 6 June 1996 and in revised form 9 December 1996)

Non-intrusive measurements of the streamwise velocity in turbulent round jets in air are performed by recording short-time displacements and distorsions of very thin tagging lines written spanwise into the flow. The lines are written by Raman-exciting oxygen molecules and are interrogated by laser-induced electronic fluorescence (RELIEF). This gives access to the spatial structure of transverse velocity increments without recourse to the Taylor hypothesis. The resolution is around 25 μm, less than twice the Kolmogorov scale η for the experiments performed (with $R_\lambda \approx 360$–600).

The technique is validated by comparison with results obtained from other techniques for longitudinal or transverse structure functions up to order 8. The agreement is consistent with the estimated errors – a few percent on exponents determined by extended-self-similarity – and indicates significant departures from Kolmogorov (1941) scaling.

Probability distribution functions of transverse velocity increments Δu over separations down to 1.8η are reported for the first time. Violent events, with Δu comparable to the r.m.s. turbulent velocity fluctuation, are found to take place with statistically significant probabilities. The shapes of the corresponding lines suggest the effect of intense slender vortex filaments.

1. Introduction

Incompressible flow allows tangential but not normal discontinuities of the velocity. Hence, it is of considerable interest to investigate *transverse* velocity increments over very small distances. By transverse we mean velocity components perpendicular to the line separating the two points, e.g. spanwise v-components with streamwise x-separation or streamwise u-components with spanwise y-separation. How small a separation ? In principle, one would like to explore separations down to the Kolmogorov dissipation scale η or even smaller. In practice, techniques used so far, which have used several probes or multi-wire probes, were restricted to separations much larger than η at high Reynolds numbers (Herweijer & Van der Water 1995; Van der Water & Herweijer 1996; Saddoughi & Veeravalli 1994) or of a few η in thick boundary layers at moderate Reynolds numbers (Vukoslavčević, Wallace & Balint 1991; Antonia 1993 and references therein).

We shall here present results obtained by Raman-excited laser-induced electronic fluorescence (RELIEF), a non-intrusive optical technique, which is applicable only to

transverse velocity increments. The results are given for separations down to about 25 μm. This is between 1.5η and 2η for the round jet used in our experiments. The RELIEF technique is presented in §2 and the experimental setup in §3. Data acquisition and processing techniques which give the spanwise variation of the streamwise velocity are described in §4. We then turn to results. Measurements of the single-point velocity distribution are presented in §5. Transverse structure functions of order two and higher are discussed in §6; this includes results which are basically validations of the RELIEF technique. Probability distribution functions (p.d.f.) of transverse velocity increments are presented in §7; this leads to the identification of strong events responsible for the tails of the p.d.f. at separations comparable to η. In the concluding §8 we discuss the nature of these events and make some remarks about future developments of the technique.

2. RELIEF: a non-intrusive technique

The RELIEF flow tagging technique is a powerful new method for non-intrusive velocity measurements in air flow (Miles, Lempert & Zhang 1991; Miles *et al.* 1993). Like its companion method PHANTOMM (photo-activated non-intrusive tracking of molecular motion), designed for use in water (Lempert *et al.* 1995; Harris *et al.* 1996), RELIEF is based on the direct tagging and tracking of an ensemble of molecules in a fluid. In the case of RELIEF, no seeding at all is necessary, as oxygen molecules themselves are tagged by changing their vibrational state and observing the advected molecules by electronic fluorescence. Arbitrary linear patterns of tagged molecules can be written in the flow using laser beams, the most straightforward being a single line. Then, at sufficiently short time intervals, the displacement of the line orthogonal to its direction is a measure of the corresponding velocity component at that point on the line. RELIEF and PHANTOMM thus directly measure flow velocities without recourse to an auxiliary effect, such as a cooling rate mechanism (e.g. with hot-wire probes) or the advection of large particles (e.g. in particle imaging velocimetry). The resolution of these methods is only limited by the time resolution between tagging and interrogation and by the spatial resolution of the optical system. Also, both RELIEF and PHANTOMM are intrinsically spatial methods, that can measure simultaneously the velocity of a large set of points in the fluid, typically along a line or grid.

The RELIEF technique is based on the vibrational excitation of oxygen molecules by stimulated Raman scattering followed by their observation by laser-induced electronic fluorescence from the Schumann–Runge band. The excitation is created by a two-photon process (at 532 and 581 nm), driving the oxygen molecules to their first vibrational level. The two-colour tagging beam is obtained from a frequency-doubled high-power (300 mJ/pulse) Q-switched Nd:YAG laser followed by a Raman cell frequency shifter that generates the 581 nm orange colour (Zhang, Lempert & Miles 1993). The duration of the tagging process is set by the laser pulse duration of 10 ns, and is thus virtually instantaneous with respect to the flow. The tagged molecules remain in their excited state for a relatively long period (of the order of 1 ms in dry air). After the tagging, the line moves with the flow for a well-defined time interval set by a precision delay generator. The tagged flow is then interrogated using a thick sheet of UV-light at 193 nm produced by an argon fluoride laser. This second pulse is also of high power (40 mJ/pulse) and of very short duration (15 ns), so that the interrogation process is also instantaneous for the flow. This ultraviolet light further excites the oxygen molecules to the Schumann–Runge band, from which they fluoresce, emitting near ultraviolet (200–400 nm) light. This fluorescence is imaged by

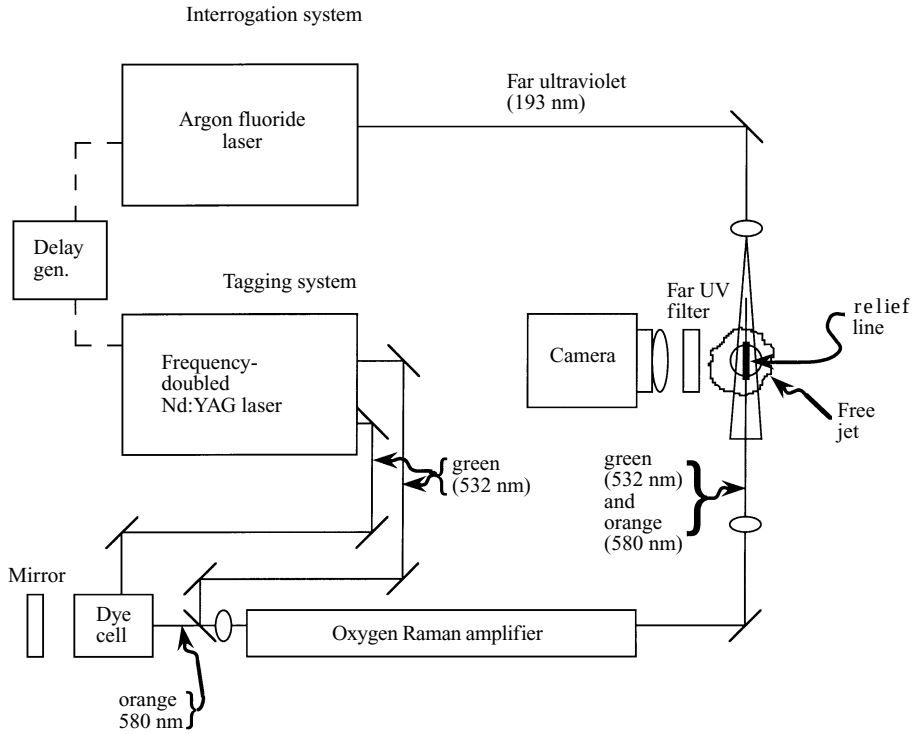

FIGURE 1. Block diagram showing the RELIEF system.

a high-sensitivity UV camera connected to a frame grabber or a video tape recorder. With the laser system used in the current experiment the lines were written and interrogated at a 5 Hz repetition rate. A block diagram of the whole RELIEF setup is shown in figure 1.

The time between tagging and interrogation has to be short compared to all relevant hydrodynamical times, so that there is no ambiguity in the velocity measurement. Short times are also important to minimize the effects of other velocity components, particularly the component along the line which otherwise may lead to an uncertainty in the exact location of the velocity element being measured. Out-of-plane motion leads to defocusing, and is not a factor with the light-collection system used for the experiment. (A second camera could be used to simultaneously image this component). Balanced against the need for a short time interval is the increased accuracy associated with a large displacement relative to the minimum resolvable displacement. In the experiments reported here, time intervals of 5 μs and 7 μs were used and found to yield virtually identical statistical properties, indicating that the time interval was not a factor. These time intervals led to displacements of a few hundred μm, allowing approximately 1 % accuracy in the absolute velocity measurement, as described in §4.

Figure 2 shows a typical example of a tagged and displaced line. The tagged lines are of the order of 100 μm wide (full width at half-maximum) and 1 cm long. Writing thinner lines would be interesting to increase the accuracy in the line centre determination, but is difficult to achieve with the current optical setup as we are already close to the diffraction limit. Also, increasing the length of the line would be necessary to measure velocities over scales close to or larger than the integral scale of the turbulent

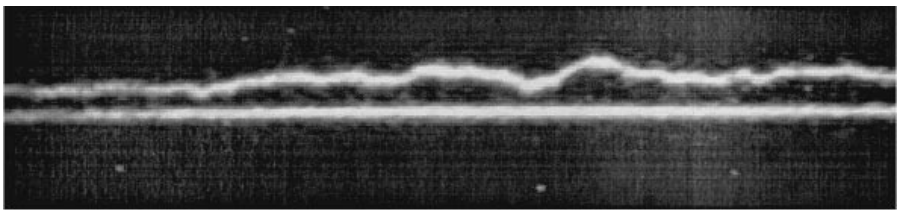

FIGURE 2. Composite image of an original tagged line and the displaced line after 7 μs in a turbulent free jet.

flow which, in our experimental setup, is typically of a few centimetres. Diffraction determines the length of the tagging line, which is quadratically proportional to the beam waist at the focus and inversely proportional to the wavelength. We thus cannot increase the length of the line or decrease its width arbitrarily; moreover, this would affect the energy density along the line and thus its brightness and the image signal-to-noise ratio. Also, the imaging camera used has a finite resolution in pixels (512 pixels in the present case), giving a limit on the ratio of scales available in our measurements. So, it is necessary with RELIEF to decide beforehand whether to investigate small scales, e.g. less than the Kolmogorov scale, using a large magnification on the camera, or to investigate large scales with a small magnification. We chose an intermediate strategy, simultaneously imaging part of the inertial-range and the dissipation-range scales, expecting to learn more by concentrating on such scales. A multi-camera system with different magnifications would certainly be feasible, but has not been implemented yet. Further developments planned will be discussed in the final section.

3. Experimental setup and main characteristics

To demonstrate the capabilities of the RELIEF technique, we have chosen to study a well-documented turbulent flow, namely a circular axisymmetric free air jet.

A circular nozzle of diameter $D = 10\,\text{mm}$ or $D = 6\,\text{mm}$ was fitted to our high-speed air flow system to obtain an axisymmetric air jet exiting freely in the laboratory. The stagnation chamber was operated at up to 70 k Pa (10 p.s.i.) higher than atmospheric pressure, leading to a pressure ratio of 1.7 between the plenum and the output. The air temperature in the plenum was about 270 K, lower than the room temperature by about 20 K, due to expansion cooling. The jet velocity at the nozzle exit was set between 270 and 200 m s^{-1} for the different experiments. This velocity is rather high, but was necessary to obtain large Reynolds numbers (typically 5×10^5 based on the jet diameter) with such a small facility; thus compressibility effects cannot be ignored at the nozzle where the Mach number is ≈ 0.8. Our measurements were performed 38 or 40 diameters downstream, so that the turbulence is fully developed (Hinze 1959). At these distances, the mean velocity has dropped to between 51 and 31 m s^{-1}, that is to Mach numbers between 0.15 and 0.1, so that compressibility effects can be safely neglected. The turbulence intensity measured by the ratio of the r.m.s. velocity fluctuations to the mean velocity was always found to be $\approx 25\,\%$, which is typical of free jets. We have chosen to report here only on six different experiments, corresponding to the longest durations and best line qualities. The main characteristics of these experiments are given in table 1. Note that experiments A and B were done on the same day with very close conditions, except for a different

Units	Nozzle ϕ (mm)	Tag pos (ϕ)	Delay (μs)	Number of lines	Line length (pixels)	$\overline{U}$ (m s^{-1})	$u_{\rm rms}$ (m s^{-1})	λ (μm)	η (μm)	R_λ
Run A	10	38	5	5617	344	48.5	12.1	686	14.4	589
Run B	10	38	7	5249	344	42.7	11.9	720	14.9	605
Run C	10	38	5	5578	344	41.6	12.7	594	13.1	534
Run D	6	40.5	7	8070	340	48.9	12.3	653	13.9	568
Run E	6	40.5	7	7885	310	51.3	12.5	622	13.5	550
Run F	6	40.5	7	10741	382	31.2	8.8	585	15.6	365

TABLE 1. Characteristics of the experiments.

delay between tagging and interrogation, to check that this factor was not affecting the measured quantities.

Let us now define the geometry of the experiment. We will denote by x the streamwise direction along the jet axis and by u the corresponding velocity component. We will use y as the spanwise coordinate along the RELIEF line which is orthogonal to the jet axis. As we are observing the displacements transverse to that line, it means that we are measuring the streamwise velocity as a function of the spanwise position, that is $u(y)$. The current RELIEF configuration does not allow the measurement of any other velocity component. The spanwise component $v(y)$ of the velocity leads to displacements of the line parallel to itself and thus cannot be observed. Furthermore, during the time interval Δt between tagging and interrogation, it shifts the point of measurement from y to $y' = y + v(y)\Delta t$. The shift may be safely ignored except when studying violent events of the sort discussed in §8. The w-component causes out-of-plane motion and leads to defocusing of the line. This is not a real problem here, as the UV sheet has a thickness of a few hundred μm, much larger than the tagging line width and the camera lens has a field depth large enough to avoid excessive blurring of the line profile. Moreover, the line centre position is not affected by defocusing. It would of course be very interesting to measure the velocity u component *along* the streamwise direction x, that is $u(x)$, to obtain simultaneously longitudinal and transverse quantities. With RELIEF, this would require a large number of parallel lines written simultaneously along the flow direction. Such a system is currently under study, using a set of mirrors to create a multipass configuration, the tagging beam being sent back and forth through the jet a large number of times. Another possibility would be to interrogate the same line many times by simply firing the UV laser more than once. This is rather hard to achieve as high-power megaHertz UV lasers in that frequency band do not exist yet, and the interrogation step also causes oxygen dissociation, significantly depleting the population of excited molecules. Furthermore, a single RELIEF line cannot be used for a very long time as it will begin to stretch and fold after a short time.

Also shown in table 1 are the measured turbulence parameters for the six experiments, namely the longitudinal Taylor microscale λ, the Kolmogorov scale η and the Taylor-scale Reynolds number R_λ. These were all estimated from the mean-square transverse velocity gradients $\left\langle \left(\partial_y u\right)^2 \right\rangle$ computed from the transverse velocity structure function as described in §6.1. Observe that the high resolution permitted by RELIEF allows an accurate measurement of y-derivatives. For an incompressible flow, assumed to be isotropic at small scales and smoothed by viscosity, we have

$\left\langle \left(\partial_y u\right)^2 \right\rangle = 2\left\langle (\partial_x u)^2 \right\rangle$. Hence,

$$\lambda = \left(\frac{2u_{\mathrm{rms}}^2}{\left\langle \left(\partial_y u\right)^2 \right\rangle} \right)^{1/2} \tag{3.1}$$

and

$$R_\lambda = \frac{\lambda u_{\mathrm{rms}}}{\nu} \tag{3.2}$$

as usual. Note that we used the standard definition of the *transverse* Taylor microscale λ_g which is also used in hot-wire experimentation, even though *longitudinal* measurements are then mostly made and isotropy is assumed to compute λ_g. The Kolmogorov scale η is obtained from the mean dissipation assuming isotropy and using (6.7). It can be seen from table 1 that R_λ stays in the range 360 to 600 in our experiments. This is not very high but dictated by the small size of our experimental facility. The Kolmogorov scale η only changes from 14 to 16 μm, having, as usual, a weak dependence on the Reynolds number.

4. The processing of RELIEF data

As described in §2, the advected RELIEF lines are imaged with a high-speed CID camera fitted with a dual microchannel plate UV image intensifier and a 2:1 fibre-optic minifier. As we are not able, for now, to do real-time (5 or 10 frames/s) processing of the RELIEF images, they are written to video tapes for later processing. This processing first involves frame digitizing with an 8-bit frame grabber attached to a workstation. From the digitized pictures, we wish to automatically extract the line displacement, that is the line centre position as a function of the coordinate along the line. We observe that the tagging linewidth at half-maximum $\approx 100\,\mu$m can be resolved with the RELIEF pixel resolution 24–28 μm, depending on the experiment. An easy way to obtain the line centre position would be, for each y-position along the line, to find the x-coordinate of the pixel of maximum brightness. This gives, however, an accuracy of only 15 % to 20 % on the velocity, which is insufficient. An improved procedure has been developed, which gives subpixel resolution and thus much more accurate velocities. It is based on the specific brightness profile of the line.

Our laser beams have a Gaussian intensity distribution since they are operated in their fundamental mode, so the projection of the beam also has a Gaussian profile. Thermal and turbulent diffusion in air lead to a very slow broadening of the line as the delay between tagging and interrogation increases (typically 5 % in 7 μs). We observe that the profile remains Gaussian for these short times. The line centre position can thus be found with subpixel accuracy by fitting a Gaussian curve to the intensity profile at each y-position along the line. Specifically, we developed a nonlinear least-square fitting routine to find the four parameters ($X_y \equiv$ line centre position, $W_y \equiv$ width, $C_y \equiv$ contrast, $B_y \equiv$ background intensity) describing the intensity profile as

$$I(x, y) = C_y \exp\left(\frac{-(x - X_y)^2}{2W_y^2} \right) + B_y \ . \tag{4.1}$$

This seems to require considerable computation, but the calculations can be very much streamlined by using a recursive evaluation of the Gaussian curve and noting that the curve parameters do not change much between adjacent pixels. So, the

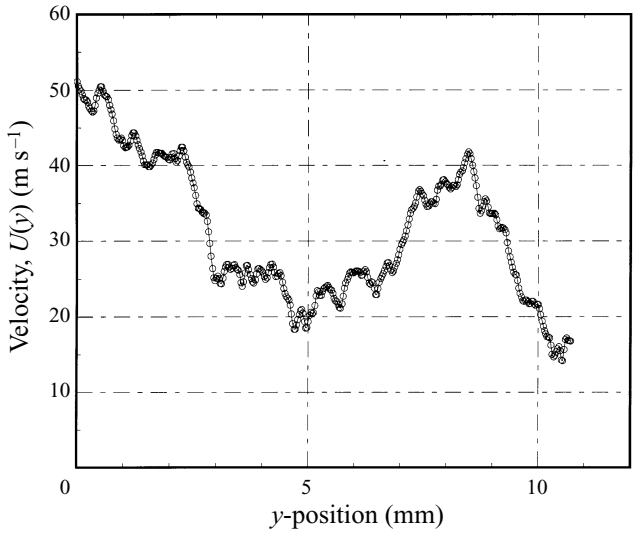

FIGURE 3. Typical velocity profile obtained by RELIEF.

fitted values for one position can be used as starting values for the next y. In this way, an optimized procedure can find all displacements X_y on a 350 pixels line in about 1.5 s with a typical accuracy of 0.1–0.2 pixels, that is 3–6 μm, leading to $\approx 1\,\%$ accuracy on the velocity. Note that this method also gives the line width W_y, which could be used to measure turbulent diffusion by increasing the delay between tagging and interrogation. For a few frames, a bright spot close to the RELIEF line (due, for example, to a dust particle) can foul the fitting routine in including the spot as part of the line. Such events can be recognized rather easily as the spot causes a large one-sided jump in the profile of the line centre position; so they are discarded before any further processing, as they would contaminate the evaluation of the velocity and, even more, of the velocity increments. The discarded lines represent a very small fraction (less than 1 %) of all data sets.

From the line centre position, we obtain immediately the velocity

$$U(y) = \frac{X_y - X_y^0}{\Delta t} \,. \tag{4.2}$$

Here, Δt is the time delay and X_y^0 is the position of the non-displaced baseline obtained by taking a few pictures with no delay between tagging and interrogation. A typical example of a velocity profile obtained by this procedure is shown in figure 3. Other examples, displaying low-probability violent events, are shown in figure 15.

From the flow velocity $U(y)$, it is then necessary to obtain the turbulent velocity fluctuations $u(y)$ by removing a 'mean' velocity. This mean velocity is a function of the spanwise coordinate y. Indeed, even close to the jet axis, the velocity profile shows measurable deviations from a flat profile. Also, slow drifts in the pressure-control system lead to temporal variations in the jet mean velocity, which are small but cannot be neglected in comparison with the turbulent velocity r.m.s. fluctuations $u_{\rm rms}$. So, we had to define a time- and position-dependent mean velocity $\overline{U}(y)$ obtained by a moving-average procedure with a period of 60 s centred on the line considered. (A similar difficulty arises when estimating slowly drifting average velocities sampled by a hot wire). With this method, the fluctuating field $u(y) = U(y) - \overline{U}(y)$ remains

homogeneous, at least to second order, its zero mean value and its r.m.s. intensity being found to vary by less than 3 % over the whole line, this being true for all data sets. This subtraction procedure also eliminates small geometric distortions of the undisplaced line due to the optics.

Statistical quantities are obtained from the velocity field $u(y)$ by a combination of time and space averaging. Since the laser's tagging frequency 5 Hz is quite low, the fields of successive lines are completely uncorrelated and time averaging reduces the variance of measurements by a factor corresponding to the number of lines N_t. Note that the RELIEF resolution is a very small fraction of the turbulence integral scale, so that the velocities of adjacent points are correlated (as they are in temporal measurements using a hot wire). Hence, the reduction in variance is much less than the number of points along the line N_y. From the discretized field $u_m \equiv u(m\rho_y)$, ρ_y being the resolution along the y-coordinate, we obtain the velocity moments as

$$\langle |u|^p \rangle = \frac{1}{N_t N_y} \sum_{\text{lines}} \sum_{m=0}^{N_y-1} |u_m|^p \ . \tag{4.3}$$

Similarly, structure functions (defined in §6 as moments of velocity increments over a distance $j\rho_y$), are determined as

$$S_p^{\perp}(j\rho_y) = \frac{1}{N_t(N_y - j)} \sum_{\text{lines}} \sum_{m=0}^{N_y-j-1} |u_{m+j} - u_m|^p \ . \tag{4.4}$$

We also estimated probability density functions (p.d.f.s) of the velocity and of velocity increments, the latter for a set of exponentially spaced separations $j = 1, 2, 4, \ldots$. The p.d.f.s were calculated by a histogram binning procedure: the interval $[-\alpha u_{\text{rms}}, \alpha u_{\text{rms}}]$ is typically divided into $\approx$ 200–250 cells of constant width† and each value of the velocity u_m or of the velocity difference $u_{m+j} - u_m$ increments the corresponding histogram bin by one. In practice, we used $\alpha \approx 6$, this value being large enough for all velocity and velocity increments to fall inside the histogram bounds. Two comments are in order here. First, even though we expected the p.d.f.s of the velocity and of the transverse velocity increments to be *symmetrical*, we systematically computed both negative and positive parts of the distribution, to check for any possible mistake in the determination of the mean velocity $\overline{U}(y)$ and also to check the accuracy in the far tails of the p.d.f.s by comparing positive and negative tails. Also, we chose to compute velocity moments and structure functions *not* from the p.d.f.s but directly from the velocity values. Indeed, the former method involves a truncation-type error, all velocity values falling in the same bin being collapsed onto the bin centre value. Note that the bin width cannot be taken too small if one wishes to reduce statistical noise on the p.d.f.s.

5. The single-point velocity distribution

One of the first things we were interested in was the velocity distribution $p(u)$, that is the single-point probability density of streamwise velocity fluctuations $u(y)$. This was estimated by the histogram binning procedure of §4 and the resulting probability densities are shown in figure 4 together with a Gaussian with r.m.s. value

† Cells with widths forming an exponential progression would provide better statistical performance with near exponential p.d.f.s of the type often found in turbulence, but they were not used here because their programming is much more involved.

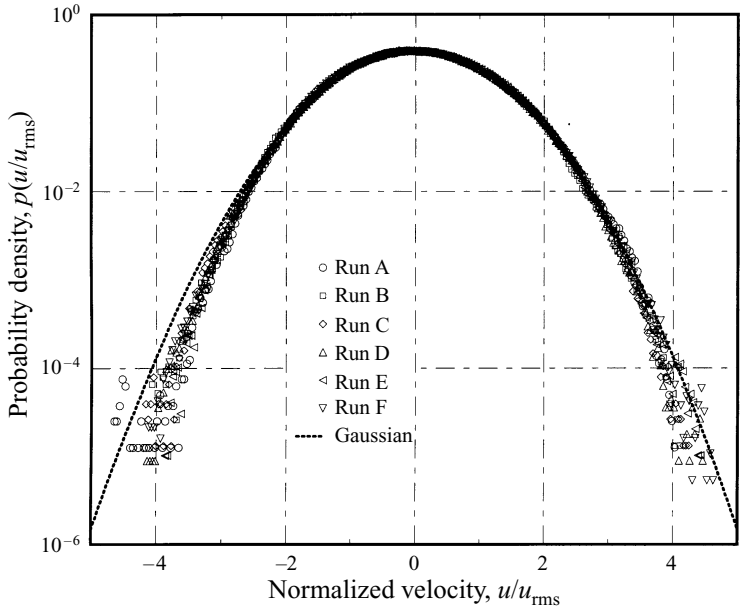

FIGURE 4. PDF of streamwise velocity normalized by $u_{\rm rms}$ for the six runs. A reference Gaussian is shown.

$u_{\rm rms} = \langle u^2 \rangle^{1/2}$. The velocity distribution is symmetrical and close to Gaussian, but not exactly so. The tails are systematically below the Gaussian value at large deviations. To check this effect, we computed the reduced moments

$$\mu_p = \frac{\langle |u|^p \rangle}{\gamma_p u_{\rm rms}^p} \,, \tag{5.1}$$

where

$$\gamma_p = \left(\frac{2}{\pi}\right)^{1/2} \int_0^\infty \mathrm{d}\xi \; \xi^p \exp\left(-\frac{\xi^2}{2}\right) = \frac{2^{p/2}}{\pi^{1/2}} \, \Gamma\left(\frac{p+1}{2}\right) \tag{5.2}$$

is the moment of order p of the absolute value of a Gaussian variable with unit variance. Results are shown in figure 5 and indicate that measured moments are always smaller than those calculated for a Gaussian distribution. The same effect was observed in numerical simulations by Jiménez *et al.* (1993 and references therein; see e.g. table 2) and no theoretical explanation for this fact has been found yet. The effect is much larger than the sampling error. Indeed, inspection of figure 4 shows that the probability density is correctly estimated up to $\pm 4 u_{\rm rms}$ and thus that moments up to order ≈ 8 should be estimated accurately.

6. Transverse structure functions

The standard definitions of longitudinal and transverse structure functions of order p are

$$S_p^{\parallel}(r) = \langle (u'(x+r) - u'(x))^p \rangle \,, \tag{6.1}$$

and

$$S_p^{\perp}(r) = \left\langle \big(u(y+r) - u(y)\big)^p \right\rangle \,, \tag{6.2}$$

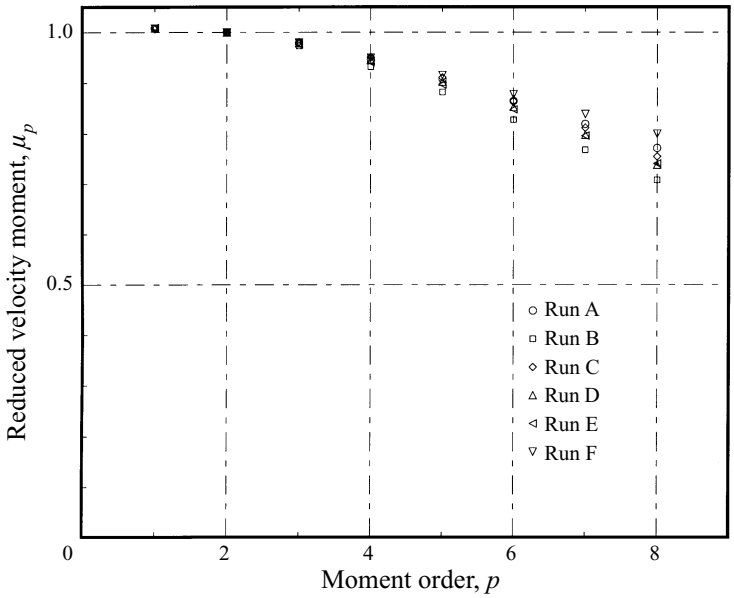

FIGURE 5. Reduced moments, as defined by (5.1), for the six runs.

respectively. In (6.1), $u'(x)$ is the longitudinal velocity fluctuation, considered now as a function of the streamwise coordinate.

For isotropic three-dimensional incompressible turbulence, the second-order longitudinal and transverse structure functions are related by (Monin & Yaglom 1975, Section 14.2)

$$S_2^{\perp}(r) = S_2^{\parallel}(r) + \frac{r}{2}\,\frac{\partial S_2^{\parallel}(r)}{\partial r}\ . \tag{6.3}$$

Furthermore, all odd-order transverse structure functions vanish. This is indeed the case for our data, within the accuracy of measurements.† Hence, we find it convenient to redefine the transverse structure function with an absolute value :

$$S_p^{\perp}(r) = \left\langle \left|u(y+r) - u(y)\right|^p \right\rangle\ . \tag{6.4}$$

We also use *reduced* transverse structure functions

$$\tilde{S}_p^{\perp}(r) = \frac{S_p^{\perp}(r)}{\gamma_p 2^{p/2} u_{\mathrm{rms}}^p}\ , \tag{6.5}$$

where γ_p is given by (5.2). The normalization is chosen in such a way that if, at very large separations r, velocity fluctuations become uncorrelated with a Gaussian p.d.f., then $\tilde{S}_p^{\perp}(r)$ goes to unity. This normalization differs from the more traditional one, in which the structure function of order p is divided by v_η^p, where $v_\eta = (\nu\varepsilon)^{1/4}$ is the 'Kolmogorov velocity'. Note that u_{rms} can be determined with better accuracy than ε or η. Furthermore, our reduced structure functions stay finite in the limit of vanishing viscosity, where both η and v_η tend to zero.

For large enough Reynolds numbers and at scales lying in the inertial range, that is much larger than the Kolmogorov scale η and much smaller than the integral scale ℓ_0,

† Odd-order transverse structure functions reduced as in (6.5) are found to be less than 10^{-3} in absolute value.

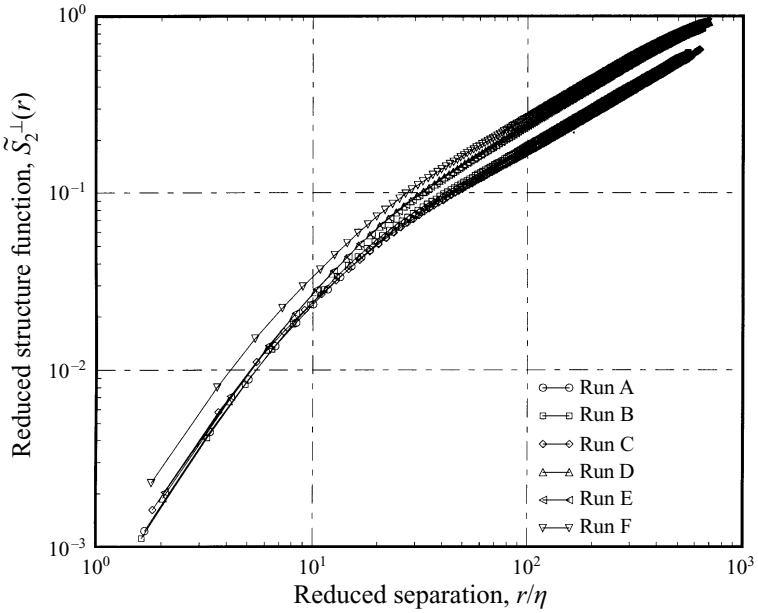

FIGURE 6. Log–log plot of the second-order transverse structure functions for the various runs, as indicated.

structure functions are found to behave approximately as power laws

$$S_p^{\parallel}(r) \propto r^{\zeta_p^{\parallel}}, \qquad S_p^{\perp}(r) \propto r^{\zeta_p^{\perp}}. \tag{6.6}$$

The scaling exponents ζ_p are the subject of much interest, as their deviation from a linear relation $\zeta_p \propto p$ would imply intermittency effects in turbulence. Also, most recent experimental works show deviations from the Kolmogorov (1941) prediction $\zeta_p^{\parallel} = p/3$. Note that there is no theoretical prediction for any transverse scaling exponent $\zeta_p^{\perp}$ except for relation (6.3).

6.1. *The second-order structure function and the Kolmogorov constant*

Figure 6 shows the second-order structure function $\tilde{S}_2^{\perp}$ *vs.* r/η for various values of R_λ. We can clearly identify a power-law inertial range at large separations and a dissipation range at scales less than about 30η. The small scales are resolved down to about 1.5η, that is, 24 μm. The dissipation scale η and the (mean) energy dissipation ε are here determined from the experimental data by the following formulas (the second of which makes use of isotropy):

$$\left\langle \left(\partial_y u\right)^2 \right\rangle = \lim_{r\to 0} \frac{S_2^{\perp}(r)}{r^2}, \qquad \varepsilon = \tfrac{15}{2}\nu \left\langle \left(\partial_y u\right)^2 \right\rangle, \qquad \eta = \left(\frac{\nu^3}{\varepsilon}\right)^{1/4}. \tag{6.7}$$

More quantitative information is obtained by measuring the 'local scaling exponent', i.e. the logarithmic derivative of the structure function, calculated here using least-square fits on octave ratios. This is shown in figure 7 for the second-order transverse structure function. It is seen that, beyond $\sim 30\eta$ and up to the largest separation available with the optical constraint mentioned in §2, the exponent becomes approximately constant. The value is around $\zeta_2^{\perp} \approx 0.7$, higher than the Kolmogorov (1941) value 2/3, but consistent with values reported by many experimentalists using either

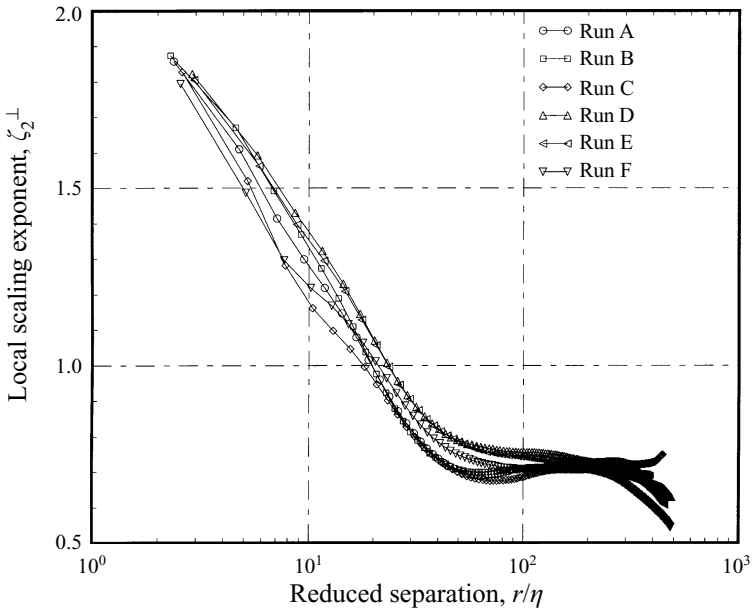

FIGURE 7. Local scaling exponent of the second-order transverse structure function for the six runs.

longitudinal or transverse second-order structure functions (Anselmet *et al.* 1984; Benzi *et al.* 1995). (Note that, by (6.3), $\zeta_2^\perp = \zeta_2^\parallel$.) At small scales the local scaling exponent rises quickly and reaches a value about 10% short of 2, the value predicted by assuming that viscosity makes the flow smooth.

The term 'Kolmogorov constant' should in principle be used exclusively to denote the constant C_2 introduced by Kolmogorov (1941) himself in connection with his two-thirds law for the second-order structure function at inertial-range separations :

$$S_2^\perp(r) = \tfrac{4}{3}\, C_2\, \varepsilon^{2/3}\, r^{2/3} \tag{6.8}$$

The 4/3 factor comes from (6.3), since C_2 (denoted C by Kolmogorov) is defined for the longitudinal structure function. It is unfortunate that the term 'Kolmogorov constant' is used more frequently to denote the constant C_K in the $k^{-5/3}$ law for the longitudinal energy spectrum, which is actually 4.02 times smaller, and has never been used by Kolmogorov. Sreenivasan (1995) gives a compilation of values of C_K from a variety of experiments with R_λ ranging from about 50 to more than 10^4. He reports values $C_K = 0.5 \pm 0.1$, corresponding to $C_2 = 2.0 \pm 0.4$. He also mentions that shear-flow turbulence usually does not display a Kolmogorov-type inertial range in the transverse spectrum until R_λ reaches values 'perhaps as high as 1000'. Our experiments suggest that R_λ values of 500 may be enough.

We measured C_2 by assuming that the second-order structure function follows exactly Kolmogorov's two-thirds law (6.8) (which produces an uncertainty of about 10%), that is by looking for a plateau in the 'compensated structure function' $r^{-2/3}\, S_2^\perp(r)$. For the six experiments A–F, we found $C_2 = 2.1 \pm 0.5$, which is consistent with Sreenivasan's (1995) data.

The fairly large scatter of data on C_2 is probably due to the fact that, because of the line-length limitation discussed in §2, the plateaus in the compensated structure functions are not very well defined, particularly at the smaller R_λ. We have also looked for other sources of errors, such as an effect of compressibility or an insufficiently

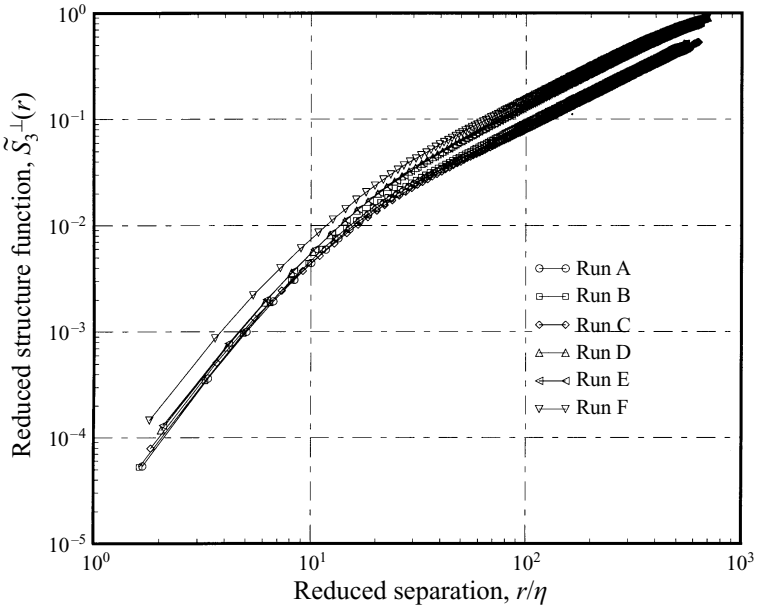

FIGURE 8. Log–log plot of the third-order structure functions.

well-resolved dissipation scale. It is known that, for subsonic flow, the corrections due to finite Mach numbers M scale as M^2. The Mach numbers based on the jet exit velocity are close to unity; those based on the mean velocity 30 diameters downstream are 0.15 or less and those based on $u_{\rm rms}$ are 0.04 or less. The latter seems the most relevant one and leads to very small compressibility corrections. Let us assume that there is an admixture of incompressible turbulence with a $k^{-5/3}$ spectrum and a small amount of acoustic turbulence with a $k^{-n_{ac}}$ spectrum. We then find that (i) when $n_{ac} > 5/3$, e.g. with a k^{-2} spectrum, the incompressible part of $S_2^{\perp}(r)$ is overestimated at inertial-range separation, while the dissipation rate ε is essentially unaffected, (ii) when $n_{ac} < 5/3$, it is the other way round. Hence, in the former case our measurements overestimate C_2 while in the latter they underestimate it. As for a poorly resolved dissipation scale, the effect should be to decrease C_2 if we assume that the graph of $S_2^{\perp}(r)$ in log–log coordinates keeps a negative curvature at the non-resolved scales.

6.2. *Higher-order structure functions*

What we have reported up to this point may be viewed as a 'standard' validation of the RELIEF technique for turbulence, that is with emphasis on second-order quantities expressible in terms of the energy spectrum. We now turn to higher-order structure functions.

Figures 8 and 9 show the transverse structure function of order 3 for all six experiments and those of order 4, 5 and 6 for experiment F, respectively. It is seen that the structure function of order p has an $r^{\zeta_p^{\perp}}$ range at separations larger than 30η. Direct measurements of the exponents $\zeta_p^{\perp}$ deteriorate rapidly when increasing the order p. This is because high-order moments of velocity increments are influenced by rare events in the tail of the corresponding p.d.f. (see e.g. Anselmet *et al.* 1984). It has been observed by Benzi *et al.* (1995) that better scaling is obtained by the extended-self-similarity (ESS) method in which the structure function of order p is plotted against the structure function of a given order p_0, rather than against the separation.

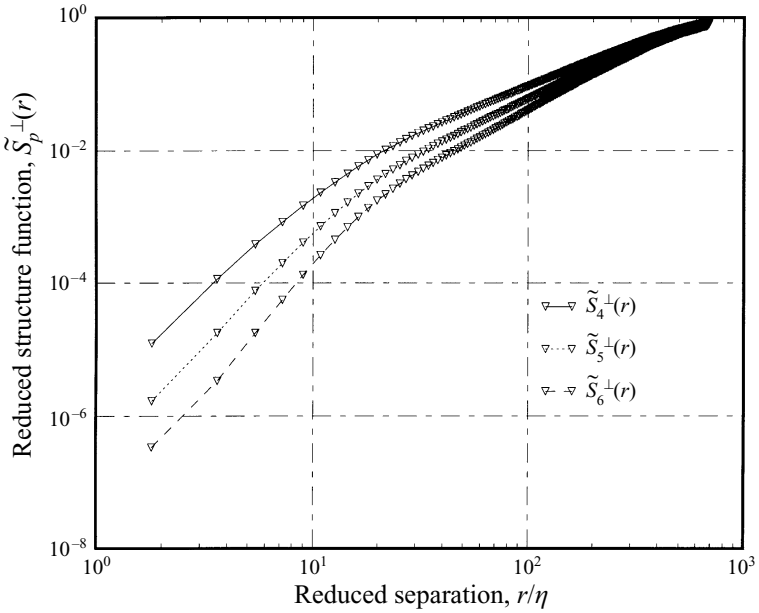

FIGURE 9. Transverse structure functions of order 4, 5 and 6 for run F.

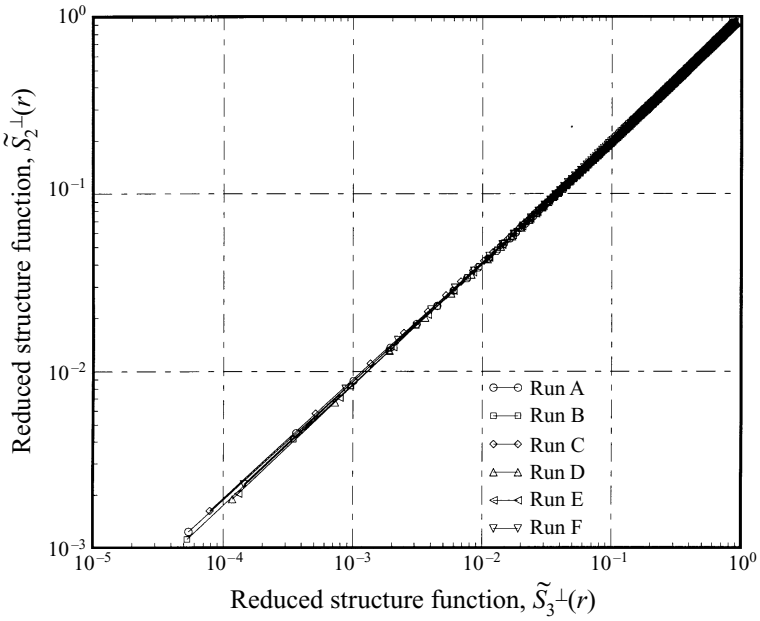

FIGURE 10. Second-order *vs.* third-order transverse structure functions (ESS method).

The choice $p_0 = 3$ is usually made, since it is known that the third-order *longitudinal* structure function has the exponent $\zeta_3^{\parallel} = 1$ (see e.g. Landau & Lifschitz 1987, §34; Frisch 1995, §6.2). There is no such constraint on the third-order transverse structure function (with an absolute value). Still, direct measurement yields here $\zeta_3^{\perp} \approx 1$ (in fact, closer to 1.02) with an accuracy better than 3 %, so that we can conveniently

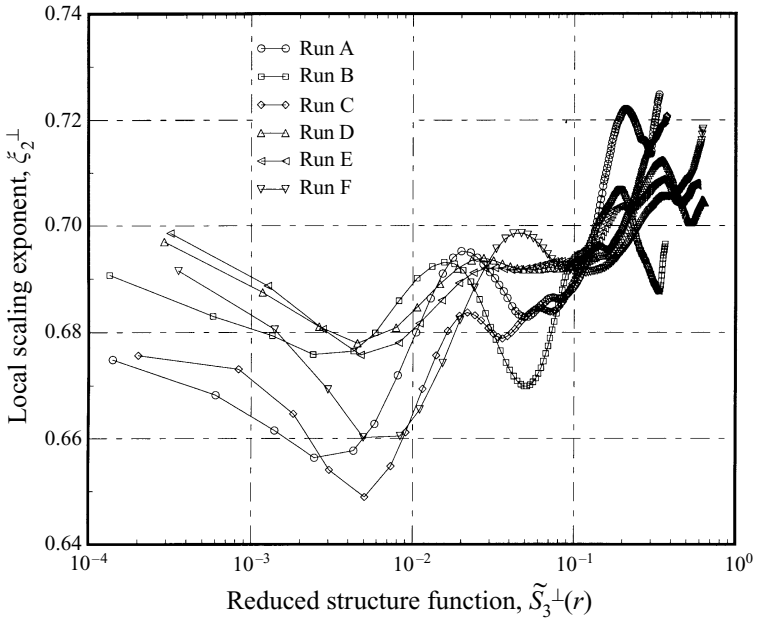

FIGURE 11. Logarithmic derivatives of $\tilde{S}_2^\perp$ with respect to $\tilde{S}_3^\perp$.

use $p_0 = 3$. Specifically, we look for an ESS scaling relation of the form

$$S_p^\perp(r) \propto \left(S_3^\perp(r)\right)^{\xi_p^\perp}, \tag{6.9}$$

thereby leaving open the possibility that $\zeta_p^\perp$ and $\xi_p^\perp$ are not exactly equal. Figures 10 and 11 show, respectively, $\tilde{S}_2^\perp$ *vs.* $\tilde{S}_3^\perp$ and the local scaling exponent $\xi_2^\perp$, defined as the logarithmic derivative of $\tilde{S}_2^\perp$ with respect to $\tilde{S}_3^\perp$. The large variance reduction brought by ESS can be appreciated by comparing these figures with figures 6 and 7. Figure 12 shows ESS plots of the transverse structure functions of order 4, 5 and 6 against the third one, for the six experiments performed. Finally, table 2 gives the exponents $\xi_p^\perp$ measured by ESS for p from 2 to 8 for the six experiments performed by least-square fits over the inertial range 20η–600η; the errors, also obtained from the least-square fits, are seen to grow, in relative value, from 1.5 % at $p = 2$ to 15 % at $p = 8$. This increase of the exponent fluctuations with the moment order p can also be observed in the local scaling exponent plots, which are not shown here because they are quite similar to figure 11 but with larger-amplitude fluctuations, reflecting the slower statistical convergence of these higher-order moments. We have enough data points to be able to determine $\xi_p^\perp$ for p up to 6 and, possibly, up to 8. These values being obtained by ESS, we changed the notation ζ_p to ξ_p. The values are clearly not all compatible with the Kolmogorov (1941) prediction $\xi_p^\parallel = p/3$. They are however consistent with the ESS values for $\xi_p^\parallel$ reported by Benzi *et al.* (1995) and also with those for $\xi_p^\perp$ reported by Van der Water & Herweijer (1996) or Kahalerras, Malecot & Gagne (1996) for $p \leqslant 8$. For higher values of p, these authors disagree on the equality of $\xi_p^\parallel$ and $\xi_p^\perp$, but a very large number of data points is necessary to get reliable estimates of moments of such high order. Note that $\xi_p^\perp$ and $\xi_p^\parallel$ need not be equal when $p \neq 2$.

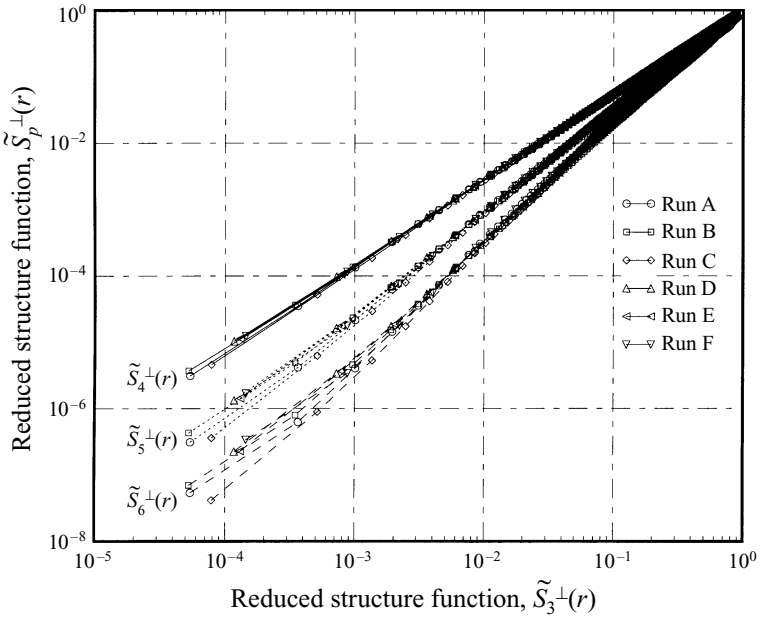

FIGURE 12. ESS plots of the transverse structure functions of order 4, 5 and 6 against the third one.

$p=2$	$p=4$	$p=5$	$p=6$	$p=7$	$p=8$
0.70 ± 0.01	1.28 ± 0.03	1.50 ± 0.05	1.75 ± 0.1	2.0 ± 0.2	2.2 ± 0.3

TABLE 2. Exponents $\xi_p^{\perp}$ of transverse structure functions for p from 2 to 8, measured by ESS.

7. PDFs of transverse velocity increments and violent events

From now on we use the following notation for transverse velocity increments:

$$\Delta u(r;y) \equiv u(y+r) - u(y). \tag{7.1}$$

The argument y will be omitted when considering statistical quantities which, by homogeneity, do not depend on y. The p.d.f. of $\Delta u(r;y)$ is denoted $p(\Delta u;r)$. PDFs are calculated as histograms using the binning method described in §4. Figure 13 shows $p(\Delta u;r)$ for three values of r/η for run F with $R_\lambda = 365$.† A Gaussian with unit variance is shown for comparison. Figure 14 shows the same results as in figure 13, but reduced using an *absolute* velocity scale $u_{\rm rms}$. Again, a Gaussian with standard deviation $\sqrt{2}u_{\rm rms}$, the r.m.s. value of Δu at very larges separations, is shown for comparison. Let us now comment on the results. The total number of points analysed is about 3×10^6 (350 per line and 5 000 to 11 000 lines). This explains why the histograms become noisy when the cumulative probability (from $-\infty$ for the negative wing and to $+\infty$ for the positive wing) drops to about 10^{-4}–10^{-5}. (Since the wings decrease very rapidly, the cumulative probability is of the same order of magnitude as the p.d.f.) Note that, in contrast to the longitudinal p.d.f., which is negatively skewed (as required by Kolmogorov's four-fifths law) the transverse

† The results being essentially identical for all the runs, we have presented only run F, to avoid cluttering the figure with data points.

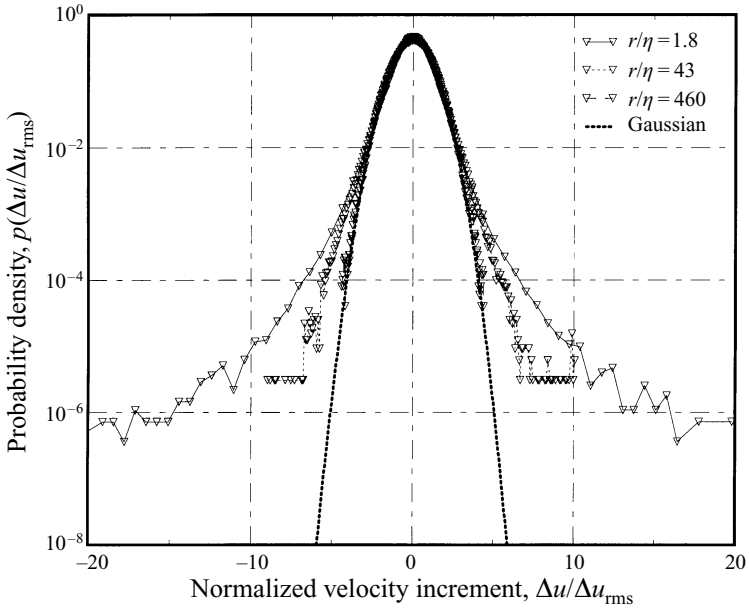

FIGURE 13. PDF of transverse velocity increments normalized by their r.m.s. value for three different separations r, as labelled.

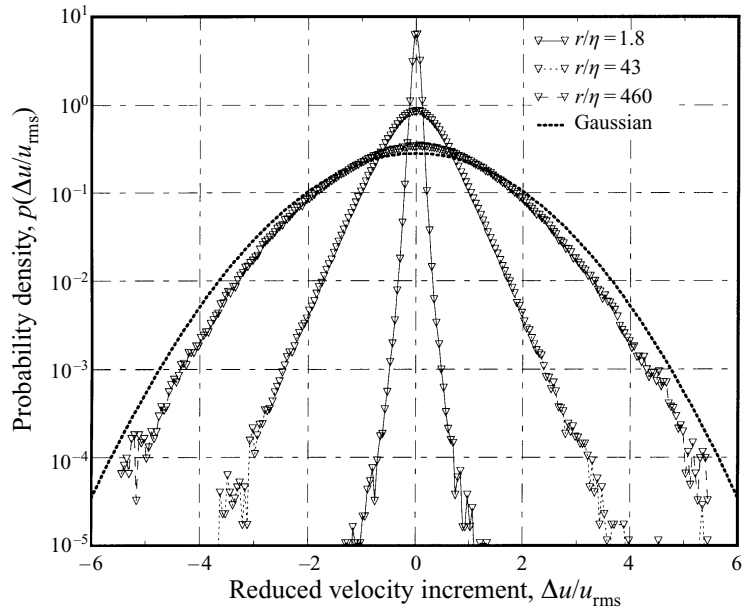

FIGURE 14. PDF of transverse velocity increments reduced by $u_{\rm rms}$. Otherwise, as in figure 13.

p.d.f. is symmetrical, except for the statistical noise. It is seen that the shape of the wings of the p.d.f. is roughly Gaussian at 460η, then roughly exponential at 43η, and finally subexponential. Qualitatively, the measured wings can be approximated by stretched exponentials $p(\Delta u; r) \propto \exp(-\alpha|\Delta u|^{\beta})$. This feature has been observed frequently for longitudinal increments (Vincent & Meneguzzi 1991) and also for

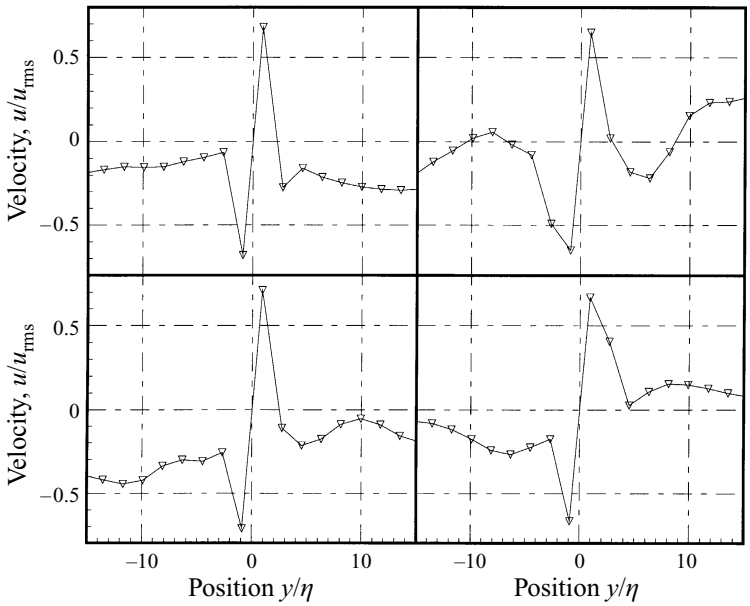

FIGURE 15. Examples of lines showing violent events. Only the neighbourhood of the violent event is shown (about 5 % of the total line length). The y- and u-origins have been shifted to the centre of the event and u has been reversed, whenever needed, to make the maximum velocity increment positive.

transverse increments (Kahalerras *et al.* 1996; Van de Water & Herweijer 1996). A simple mechanism leading to p.d.f.s with stretched exponential tails by multiplication of independent random variables has been proposed by Frisch & Sornette (1996). We must, however, stress that stretched exponential behaviour with $\beta < 2$ cannot hold for arbitrarily large arguments Δu if the single-point p.d.f. falls off as a Gaussian or faster, as suggested by figure 4. Indeed, in the Appendix, we prove that, irrespective of the value of the increment r, the probability of having a velocity increment $\Delta u > v$ cannot exceed twice the probability of having a single-point velocity fluctuation $u > v/2$. Loosely expressed, the p.d.f. of velocity increments cannot cross (a suitable multiple of) the single-point p.d.f.

What, to the best of our knowledge, has never been observed before is the p.d.f. of transverse increments with such a small separation, namely 1.8η, that is 28 μm, the pixel size for run F. A remarkable feature, seen on figure 14, is that transverse velocity increments of about $0.5\,u_{\rm rms}$ across a distance of 1.8η are within the statistically significant range where the probability is $\geqslant 10^{-4}$. We note that, for separations of 9η, Van der Water & Herweijer (1996) reported transverse increments of a few $u_{\rm rms}$ with well-defined probabilities and also observed occasional events with increments of up to $8\,u_{\rm rms}$. We shall leave the discussion of the meaning and consequences of such 'violent events' to the next section. In order to check for their possibly spurious character, we have developed a procedure to identify the lines responsible for such events. For each of the six runs, we associate to each of the 5 000 to 11 000 collected lines its maximum velocity excursion, defined as the absolute value of the largest velocity change between adjacent measurement points, the separation being typically $(1.5\text{–}1.8)\,\eta$. We then extract the twenty lines having the largest velocity excursions. Figure 15 shows the four strongest events from run F. Note that (i) as described in §4, a small number (less than 1 %) of lines with unacceptably discontinuous profiles

have been discarded before any processing, (ii) more than 75 % of our violent events show both a positive and a negative excursion ; so we can be reasonably sure that these 'violent events' are real and are not artifacts produced by the data acquisition or its processing.

8. Concluding remarks

We have applied RELIEF to non-intrusive probing of a turbulent jet down to scales of about 25 μm. The results for the second-order transverse structure function (related to the longitudinal structure function by (6.3)) are in qualitative and quantitative agreement with well-documented results for jets of much larger size but comparable R_λ values. Our exponents for transverse structure functions of order 3 to 8, measured with an accuracy of a few percent, do not show any significant departures from the values reported in the literature for longitudinal structure functions.

Using RELIEF we have identified violent transverse events with velocity increments comparable to $u_{\rm rms}$ over distances comparable to the Kolmogorov dissipation scale η. The identification of lines associated to individual events (cf. end of §7) indicates that a large fraction of them are not spurious. The associated shapes (cf. figure 15) are not consistent with a thin vortex sheet, for which the velocity should exhibit some kind of step. A good candidate is a *slender vortex filament* with a core diameter of about η and a circulation of about $\eta u_{\rm rms}$. Assuming that the filament has an essentially straight axis, that the tagging line does not intersect the core and that the orientation is arbitrary, a simple calculation gives the following contribution to the streamwise velocity profile (after a suitable translation in y) :

$$u(y) = \frac{\alpha y + \beta}{y^2 + \gamma^2}. \tag{8.1}$$

(We have here ignored the distorsion in the profile due to the fact that the point of measurement is at $y' = y + v(y)\Delta t$.) If the axis approaches the tagging line by an amount $O(\eta)$, then the maximum transverse velocity increment is $O(u_{\rm rms})$ and the width of the profile $O(\eta)$. Note that $u(y)$ decreases as $1/y$ for large y. The longitudinal contribution has a different functional form (corresponding to $\alpha = 0$ in (8.1)) and decreases as $1/y^2$, as observed in a calculation similar to ours made by Belin *et al.* (1996). It also follows from their calculation that the longitudinal velocity signal will only show a one-sided excursion unless the filament passes very close to the probe ; also, the amplitude of the excursion is reduced by the factor $v/\overline{U}$ which must be small for the Taylor hypothesis to be valid. Thus transverse probing is much more favourable for detecting vortex filaments.† We observe that the frequency of events having velocity increments comparable to $u_{\rm rms}/2$ is consistent with the following picture : within a volume of the order of the integral scale cubed, there is typically one such filament with a core diameter $O(\eta)$, a circulation $O(\eta u_{\rm rms})$ and a length comparable to the integral scale. Alternatively, the filaments could be shorter and more numerous, as is the case for the 'worms' described by Jiménez *et al.* (1993).

RELIEF, and its companion method PHANTOMM for operating in a liquid (see e.g. Lempert *et al.* 1995; Harris *et al.* 1996), have the advantage that they can measure transverse velocity increments over distances at least one order of magnitude smaller than anything that can be done with intrusive techniques. The present limitation of 25 μm should be reducible to approximately 5 μm using higher magnification and

† With a single hot-wire probe, a transverse event with a velocity excursion $\sim u_{\rm rms} \ll \overline{U}$ will be mistaken for a longitudinal event of strength $(1/2)u_{\rm rms}^2/\overline{U}$.

thinner lines. Work is currently under way to increase the brightness of the lines by interrogating higher vibrational states that have been populated by collisional energy transfer, and this will further improve the capability of using RELIEF at higher resolution (Diskin, Lempert & Miles 1996).

Future improvements to RELIEF will also concentrate on higher brightness lines through the use of new lasers for the interrogation step. This will improve the signal-to-noise ratio and allow us to operate at lower densities. The system is now being modified for operation with large-scale facilities. Particular attention is being given to the development of a portable device with large-scale optics, so lines can be interrogated at distances up to several metres from the collection optics.

With spatial resolutions extending from the large scale down to more than one order of magnitude finer than anything achieved previously, RELIEF is opening up new windows on turbulence, and could reveal structures even smaller than current models can predict.

Thanks are due to B. Castaing, Y. Gagne, S. A. Orszag, A. Pumir, Z. S. She, P. Tabeling and V. Yakhot for helpful comments. This work was supported by the National Science Foundation (grant CTS92-12457), the Direction des Recherche et Moyens Techniques (grant 94/2582) and by a NATO Collaborative Research Grant (grant CRG.920480).

Appendix. A bound for the p.d.f. of increments

Let us denote by $p(u)$ and $p(\Delta u; r)$ the single-point p.d.f. and the p.d.f. of velocity increments Δu over a distance r, respectively. We assume that the velocity is homogeneous and we claim that, for any r, we have

$$\begin{aligned}\text{Prob}\,\{|\Delta u| > v\} &\equiv \int_{|\Delta u|>v} p(\Delta u; r)\,\mathrm{d}\Delta u \\ &\leqslant 2\,\text{Prob}\,\left\{|u| > \tfrac{1}{2}v\right\} \equiv 2\int_{|u|>v/2} p(u)\,\mathrm{d}u. \end{aligned} \tag{A 1}$$

Indeed, writing $\Delta u = u(y+r) - u(y)$, we observe that $|\Delta u| > v$ requires that at least one of the two terms $u(y+r)$ or $u(y)$ be larger than $v/2$. Hence,

$$\begin{aligned}\text{Prob}\,\{|\Delta u| > v\} &\leqslant \text{Prob}\,\left\{|u(y)| > \tfrac{1}{2}v \;\text{ or }\; |u(y+r)| > \tfrac{1}{2}v\right\} \\ &\leqslant \text{Prob}\,\left\{|u(y)| > \tfrac{1}{2}v\right\} + \text{Prob}\,\left\{|u(y+r)| > \tfrac{1}{2}v\right\}. \end{aligned} \tag{A 2}$$

By the assumed homogeneity, the two terms on the right-hand side of (A 2) are equal. This proves (A 1). Now, in the case of p.d.f.s $p(x)$ with an exponential or stretched exponential tail, the cumulated probability $\text{Prob}\,\{|z| > x\}$ and $p(x)$ differ only by algebraic prefactors for large values of the argument x. It follows from this and (A 1) that, for example, if $p(u)$ is Gaussian, then $p(\Delta u; r)$ cannot be a stretched exponential with an exponent less than 2 for arbitrarily large values of the argument Δu.

REFERENCES

ANSELMET, F., GAGNE, Y. HOPFINGER, E. J. & ANTONIA, R. A. 1984 High-order velocity structure functions in turbulent shear flow. *J. Fluid Mech.* **140**, 63–89.

ANTONIA, R. A. 1993 Direct numerical simulations and hot wire experiments: a possible way ahead? In *New Approaches and Concepts in Turbulence* (ed. Th. Dracos & A. Tsinober), pp. 349–365. Birkhäuser, Basel.

Belin, F., Maurer, J., Tabeling, P. & Willaime, H. 1996 Observation of intense filaments in fully developed turbulence. *J. Phys. Paris* II **6**, 573–584.

Benzi, R., Ciliberto, S., Baudet, C. & Ruiz Chavarria, G. 1995 On the scaling of three dimensional homogeneous and isotropic turbulence. *Physica* D **80**, 385–398.

Diskin, G. S., Lempert, W. R. & Miles, R. B. 1996 Observation of vibrational relaxation dynamics in $X^3\Sigma_g^-$ Oxygen following stimulated Raman excitation to the $v = 1$ level: implications for the RELIEF flow tagging technique, *AIAA Paper* 96-0301.

Frisch, U. 1995. *Turbulence: the Legacy of A. N. Kolmogorov*. Cambridge University Press.

Frisch, U. & Sornette, D. 1997 Extreme deviations and applications. *J. Phys. Paris* II (submitted).

Harris, S. R., Lempert, W. R., Hersch, L., Burcham, C. L., Saville, D. A., Miles, R. B., Gee, K. & Haugland, R. P. 1996 Quantitative measurements of internal circulation in droplets using flow tagging velocimetry. *AIAA J.* **34**, 449–454.

Herweijer, J. A. & Van der Water, W. 1995 Transverse structure functions of turbulence. In *Advances in Turbulence* V (ed. R. Benzi), pp. 210–216. Kluwer.

Hinze, J. O. 1959 *Turbulence*. McGraw-Hill.

Jiménez, J., Wray, A. A., Saffman, P. G. & Rogallo, R. S. 1993 The structure of intense vorticity in isotropic turbulence. *J. Fluid Mech.* **255**, 65–90.

Kahalerras, H., Malecot, Y. & Gagne, Y. 1996 Transverse structure functions in three-dimensional turbulence. In *Advances in Turbulence* VI (ed. S. Gavrilakis, L. Machiels & P. Monkewitz), pp. 235–238. Kluwer.

Kolmogorov, A. N. 1941 Dissipation of energy in locally isotropic turbulence. *Dokl. Akad. Nauk SSSR* **32**, 16–18.

Landau, L. D. & Lifschitz, E. M. 1987 *Fluid Mechanics*, 2nd edn. Pergamon.

Lempert, W. R., Magee, K. Ronney, P., Gee, K. R. & Haugland, R. P. 1995 Flow tagging velocimetry in incompressible flow using photo-activated nonintrusive tracking of molecular motion (PHANTOMM). *Exps. Fluids* **18**, 249–257.

Miles, R. B., Lempert, W. & Zhang, B. 1991. Turbulent structure measurements by RELIEF flow tagging. *Fluid Dyn. Res.* **8**, 9–17.

Miles, R. B., Zhou, D., Zhang, B., Lempert, W. R. & She, Z.-S. 1993 Fundamental turbulence measurements by RELIEF flow tagging. *AIAA J.* **31**, 447–452.

Monin, A. S. & Yaglom, A. M. 1975 *Statistical Fluid Mechanics*, vol. 2. MIT Press.

Saddoughi, S. G. & Veeravalli, S. V. 1994 Local isotropy in turbulent boundary layers at high Reynolds numbers. *J. Fluid Mech.* **268**, 333–372.

Sreenivasan, K. R. 1995. On the universality of the Kolmogorov constant. *Phys. Fluids* **7**, 2778–2784.

Van der Water, W. & Herweijer, J. A. 1996 High-order structure function of turbulence. *J. Fluid Mech.* (submitted).

Vincent, A. & Meneguzzi, M. 1991. The spatial structure and statistical properties of homogeneous turbulence. *J. Fluid Mech.* **225**, 1–25.

Vukoslavčević, P., Wallace, J. M. & Balint, J.-L. 1991 The velocity and vorticity vector fields of a turbulent boundary layer. Part 1. Simultaneous measurement by hot-wire anemometry. *J. Fluid Mech.* **228**, 25–51.

Zhang, H., Lempert, W. R. & Miles, R. B. 1993 Efficient vibrational Raman conversion in O_2 and N_2 cells by use of superfluorescence seeding. *Optics Lett.* **18**, 1132–1134.